Inner-shell capture using atomic potentials: A distorted strong-potential Born treatment

Steven Alston
Physics Department, Pennsylvania State University, Wilkes-Barre Campus, Lehman, Pennsylvania 18627
(Received 14 January 1993)

The influence of a distorted nuclear motion on electron capture from the inner shells of atoms, when atomic model potentials, rather than scaled Coulomb potentials, are used in the motion of the active target electron, is investigated in the distorted strong-potential Born approximation to the exact capture amplitude. A comparison is made with the earlier undistorted strong-potential Born approximation and other theories, and with experiment. The modification of the impulse-approximation cross section is shown to be generally much less in the distorted theory and is shown to give quite good agreement with the experimental data. At energies below the peak in the capture cross sections, the present results show significantly better agreement with experiment and also good agreement with the recent coupled-Sturmian-pseudostate results of Winter [Phys. Rev. A **47**, 264 (1993)], who used the same atomic model potential.

PACS number(s): 34.70.+e

I. INTRODUCTION

At intermediate collision energies, a consistent, accurate treatment of electron capture from the inner shells of atoms has proven more difficult to obtain than has a comparable theory for ionization. This owes largely to the rearrangement nature of the process and, within a perturbative framework, to the long-range nature of the Coulomb interactions between each pair of particles. However, for capture by light projectiles such as protons, two aspects of the problem allow simplification of the treatment. First, the charge of the projectile can be taken to be small relative to the charge of the heavy target nucleus, implying that a consistent approach can rely on a simple first-order treatment of the electron-projectile interaction if also the dynamics of the electron is described using the strong electron–target-nucleus interaction. Second, the orbital velocity of the electron in the final bound state can be assumed small relative to the incident projectile velocity. This permits the sum over intermediate states of the target, representing the time development of the electronic wave function, to be collapsed to a single term corresponding to ionization of the target electron.

Such a theory, the strong-potential Born approximation, was developed a decade ago [1,2]. While the agreement of calculated total cross sections with experiment was encouraging [3,4], it was pointed out that the exact version of this amplitude contained a nonintegrable singularity [5], derived from the elastic-channel scattering contribution, which clearly made justification of any approximate, but more intuitive and tractable, version of the theory problematic. It was noted, however, that the problem was of a rather spurious nature which could be corrected by a proper treatment of elastic-channel scattering [6]. Yet, the intimate connection of this problem with the long-range behavior of the two-body Coulomb interactions meant that a formally consistent revision of the theory was necessary. Over the last few years, within a distorted-wave theory of scattering amplitudes, this *distorted* strong-potential Born approximation (DSPB) has been developed by Taulbjerg, Barrachina, and Macek [7,8].

A key aspect of the DSPB amplitude is its use of initial- and final-channel distortion potentials built up from the active-electron–projectile and active-electron–target-core interactions. In a multielectron target, the latter takes on a very different form asymptotically than the bare-nucleus form which exists in the inner region. The DSPB theory developed in this paper incorporates a realistic representation of the interaction. To good approximation, the interaction can be approximated by a local potential. An analytic, one-electron model potential due to Green, Sellin, and Zachor is used in the present work [9]. The potential smoothly matches the electron–bare-nucleus interaction at small distances with the electron–singly-charged-ion interaction at large distances. It depends on two parameters which are optimized for each atom and are available for a wide range of atoms (and ions) [10].

As already noted, the model potential is used to define the final-channel distortion potential in the DSPB amplitude. The use of this potential in the amplitude primarily distinguishes the DSPB amplitude from the original SPB amplitude. The present work also extends the initial study [8] by going beyond the limited, so-called full-peaking approximation used in the previous evaluation of the amplitude.

An exact numerical calculation of the DSPB amplitude is extremely difficult and is not attempted here. Rather, the focus is on obtaining the first calculations with the theory using a realistic atomic potential for the target. An approximate evaluation of the amplitude is presented which relies on the smallness of the binding energy of the captured electron relative to its outgoing kinetic energy, and on the fact that the minimum momentum transfer is of the order of the large impact velocity [3]. A near-the-energy-shell approximation [11] to the propagation of the

electron in the strong field near the target nucleus (where capture from inner shells predominantly occurs) introduces errors only of the order of the square of the ratio of the nuclear charges to the impact velocity. In addition, an eikonal approximation to the heavy-particle motion is made which introduces only very small errors of the order of the ratio of the electron mass to either of the heavy-particle masses.

Considerable experimental data exist for capture from the inner shells of atoms. A comparison will be made with experimental results for protons incident on carbon, neon, and argon atoms [12–15]. Much effort has also gone into obtaining other theoretical descriptions of inner-shell capture, including the continuum distorted-wave approximation (CDW) [16,17] and a renormalized version of the strong-potential Born approximation (RSPB) [18]. At the intermediate velocities treated, coupled-state calculations are also possible, and a comparison is made with such work for carbon, neon, and argon [19–21].

The plan of the paper is the following. The DSPB formalism is introduced in Sec. II. In Sec. III, details of the evaluation of the amplitude are discussed with reference to a specific atomic model potential and its incorporation in the final distorting potential. Section IV presents the calculated results and compares them with experimental results and other theoretical results. Concluding remarks are made in Sec. V. An appendix on off-energy-shell scattering is also given. Atomic units are used unless otherwise noted. A plane-wave state $\phi_{\mathbf{k}}$ of momentum $\mathbf{k}$ represented in coordinate space $\mathbf{r}$ is normalized as $\phi_{\mathbf{k}}(\mathbf{r})=e^{i\mathbf{k}\cdot\mathbf{r}}$.

II. DISTORTED STRONG-POTENTIAL BORN APPROXIMATION

We consider a collision between particles in which a single electron can be taken as participating in the dynamics. Generally, the target ion and possibly the projectile ion may contain nonactive electrons, although the results presented here will focus on a bare projectile ion. In this one-active-electron, three-body model scattering problem, a projectile ion P impacts on a target consisting of the active electron e and a target ion T. The two-body interactions between each pair of particles are of modified Coulomb form (which includes the pure Coulomb form as a special case). The collision is assumed asymmetric so that the projectile charge Z_P is much smaller than the target nuclear charge Z_T. The collision process is

$$P+(T+e)\rightarrow(P+e)+T \ ,$$

where the parentheses denote bound electron-ion partners.

Since the two-body interactions are Coulombic asymptotically and since the projectile and target ions are much heavier than the electron, a distorted-wave theory of scattering amplitudes [22] is employed together with an eikonal approximation for the heavy-particle motion. The development in this section closely follows the treatment of Taulbjerg, Barrachina, and Macek [8] (including their Appendix A). The reader is referred there for greater detail.

As a result of the eikonal approximation, the initial and final perturbations reduce to single interactions,

$$V_i=V_{Pe}(\mathbf{r}_P), \quad V_f=V_{Te}(\mathbf{r}_T) \ , \tag{1}$$

where $\mathbf{r}_P$ and $\mathbf{r}_T$ denote the electron's position relative to the projectile-ion and target-ion centers of mass, respectively. Corresponding to these potentials are the distorting potentials U_i and U_f for the initial and final scattering channels. The major extension of the present work is the explicit incorporation of effects arising from the nonactive electrons. For inner-shell processes, the orbital velocities of the outer electrons are small compared with that of the K-shell electron. The orbital velocity of the $2s$ electron is approximately one-fourth of that for the $1s$ electron, even for the least asymmetric case of proton-carbon collisions considered here [23]. Therefore the effects of the outer electrons on the collision can be incorporated in an averaged and static manner by means of a screened electron–target-ion (or electron–projectile-ion) potential. The inclusion of explicit multielectron processes is beyond the scope of the present treatment. The asymptotic behaviors of the potentials in Eq. (1) are

$$\begin{aligned} V_{Pe}(\mathbf{r}_P)&\sim -Z_P^{\infty}/r_P \ , \\ V_{Te}(\mathbf{r}_T)&\sim -Z_T^{\infty}/r_T \ . \end{aligned} \tag{2}$$

For neutral target atoms $Z_T^{\infty}=1$, and for incident protons $Z_P=Z_P^{\infty}=1$. The representation of the screening in V_{Te} for smaller radii is discussed in Sec. III C.

The transition amplitude for electron transfer is

$$A=\langle \Psi_f^- | V_{Pe}-U_i | \Phi_i^+ \rangle \ , \tag{3}$$

which is still exact except for terms of the order of the electron mass divided by the heavy-particle masses [21]. The incoming-wave final scattering state Ψ_f^- is defined by the Lippmann-Schwinger equation

$$|\Psi_f^-\rangle \equiv [1+G^-(V_{Te}-U_f)]|\Phi_f^-\rangle \ , \tag{4}$$

where G^- is the exact Green operator for the collision and Φ_f^- is the final asymptotic scattering state defined in coordinate representation by

$$\langle \mathbf{r}_P,\mathbf{R}_P|\Phi_f^-\rangle=\phi_{\mathbf{K}_f}(\mathbf{R}_P)D_{\mathbf{K}_f}^-(\mathbf{R}_P)\phi_f(\mathbf{r}_P) \ . \tag{5}$$

The function $D_{\mathbf{K}_f}^-(\mathbf{R}_P)$ represents the distortion of the heavy-particle plane-wave motion arising both from the asymptotic Coulomb behavior of the interaction and from the short-range screening of the nonactive electrons.

To specify the distortion function sufficiently for later purposes, an eikonal approximation is introduced:

$$D_{\mathbf{K}_f}^-(\mathbf{R})=(vR+\mathbf{v}\cdot\mathbf{R})^{iZ_T^{\infty}/v} \times\exp\left\{-\frac{i}{v}\int_Y^{\infty}dY'\left[U_f(R)+\frac{Z_T^{\infty}}{R}\right]\right\} . \tag{6}$$

The lower limit of the integral is $Y=-\mathbf{R}\cdot\hat{\mathbf{v}}$, with $\mathbf{v}$ the incident projectile velocity [21]. (A caret denotes a unit vector.) The initial asymptotic scattering state in the coordinate representation is similarly defined as

$$\langle \mathbf{r}_T, \mathbf{R}_T | \Phi_i^+ \rangle = \phi_{\mathbf{K}_i}(\mathbf{R}_T) D^+_{\mathbf{K}_i}(\mathbf{R}_T) \phi_i(\mathbf{r}_T) \ . \quad (7)$$

In these functions, the position of the projectile relative to the target center of mass is denoted by $\mathbf{R}_P$, the position of the target ion relative to the projectile-ion–electron center of mass is denoted by $\mathbf{R}_T$, and the initial and final heavy-particle wave vectors are $\mathbf{K}_i$ and $\mathbf{K}_f$. The initial and final bound-state wave functions are ϕ_i and ϕ_f, respectively.

The distortion functions are determined by specifying the distorting potentials U_i, U_f. The forms used in the present study represent a minimal choice based on the bound-state static charge distributions, and are consistent with the known asymptotic behaviors of the electron-ion potentials. The initial- and final-channel distorting potentials are defined as

$$U_i(\mathbf{R}_T) = \int d\mathbf{r}_T |\phi_i(\mathbf{r}_T)|^2 V_{Pe}(\alpha \mathbf{r}_T - \mathbf{R}_T) \ , \quad (8a)$$

$$U_f(\mathbf{R}_P) = \int d\mathbf{r}_P |\phi_f(\mathbf{r}_P)|^2 V_{Te}(\beta \mathbf{r}_P + \mathbf{R}_P) \ . \quad (8b)$$

The relations between the electronic coordinate vectors have been inserted here with the mass ratios $\alpha \equiv M_T/(m+M_T) \approx 1$ and $\beta \equiv M_P/(m+M_P) \approx 1$, where m is the electron mass and M_P and M_T are the projectile- and target-ion masses, respectively. The influence of the nonactive electrons on the dynamics of the collision appears in the functional form of the electron–target-ion potential V_{Te} and in U_f through its dependence on V_{Te}.

In the interaction region, $r_T \lesssim 1/Z_T$, predominantly leading to capture, the electron–target-ion interaction is much stronger than the electron–projectile-ion interaction. Account is thus taken in the exact Green operator only of the propagation in the strong target field [1]. In the expansion of the exact Green operator in the weak potential, the leading term is the target Green operator G_T^-:

$$G^- \approx G_T^-(E) = \left[E + \frac{1}{2\nu_i} \nabla^2_{\mathbf{R}_T} + \frac{1}{2\mu} \nabla^2_{\mathbf{r}_T} - V_{Te}(r_T) - i\eta \right]^{-1} , \quad (9)$$

where the internal reduced mass is $\mu = mM_T/(m+M_T) \approx m$, the full three-body reduced mass is $\nu_i = M_P(m+M_T)/(m+M_P+M_T) \approx M_P M_T/(M_P+M_T)$, and η is an infinitesimal quantity. The total energy of the system is given by $E = (1/2\nu_i)K_i^2 + \varepsilon_i = (1/2\nu_f)K_f^2 + \varepsilon_f$. The initial and final bound-state energies are ε_i and ε_f, respectively, and $\nu_f = M_T(m+M_P)/(m+M_P+M_T)$. The resulting distorted strong-potential Born scattering state is given by

$$|\Psi_f^-\rangle \approx |\Psi^-_{\mathrm{DSPB}}\rangle \equiv [1 + G_T^-(V_{Te} - U_f)]\Phi_f^-\rangle \ . \quad (10)$$

Since the function $D^+_{\mathbf{K}_i}(\mathbf{R}_T)$ depends on the distorting potential U_i, the amplitude Eq. (3) still contains higher-order contributions in the weak potential V_{Pe}. In a consistent strong-potential approximation, these are neglected:

$$\langle \mathbf{r}_T, \mathbf{R}_T | \Phi_i^+ \rangle \approx \phi_{\mathbf{K}_i}(\mathbf{R}_T) \phi_i(\mathbf{r}_T) \ . \quad (11)$$

In the evaluation of the DSPB amplitude [Eq. (3) with Eq. (11)], the *short-range* nature of the initial-channel perturbation $V_{Pe} - U_i$ ensures that the nonintegrable singularity which is present in the undistorted version of the theory [5] does not arise here. Alternatively, it can be shown that the elastic-channel pole contribution of V_{Pe} is canceled exactly by the U_i contribution.

An explicit form for the distorted strong-potential Born scattering state can be obtained by using the identity $G_T^-(V_{Pe} + U_f - V_{Te})|\Phi_f^-\rangle = |\Phi_f^-\rangle$, derived by Faddeev [24,8]. Introduce Fourier analyses of the functions $D^-_{\mathbf{K}_f}(\mathbf{R}_P)$ and $\phi_f(\mathbf{r}_P)$ in Eq. (5), write $\mathbf{R}_P = (1-\alpha\beta)\mathbf{r}_T + \beta \mathbf{R}_T$ [25], and relate the transform of the product of the potential and bound-state wave function to the transform of the wave function itself $[\widetilde{V_{Pe}\phi_f}](\mathbf{k}) = \Delta\varepsilon \tilde{\phi}_f(\mathbf{k})$, where $\Delta\varepsilon = \varepsilon_f - \frac{1}{2}k^2 \neq 0$. One derives

$$\langle \mathbf{r}_T, \mathbf{R}_T | \Psi^-_{\mathrm{DSPB}} \rangle = (2\pi)^{-3/2} \int d\mathbf{k}\, d\mathbf{S}\, \tilde{\phi}_f(\mathbf{k}) \tilde{D}^-_{\mathbf{K}_f}(\mathbf{S}) \times \frac{\Delta\varepsilon}{\Delta\varepsilon - \mathbf{v}\cdot\mathbf{S}} \psi^-_{\varepsilon_S, \mathbf{k}+\mathbf{v}}(\mathbf{r}_T) \times \phi_{\beta\mathbf{K}_f - \mathbf{k} + \mathbf{S}}(\mathbf{R}_T) \ . \quad (12)$$

(A tilde over a function denotes a Fourier-transformed quantity.) The off-energy-shell electronic scattering wave function is defined as

$$\psi^-_{\varepsilon_S, \mathbf{k}+\mathbf{v}}(\mathbf{r}_T) \equiv \frac{(\varepsilon_S - \frac{1}{2}|\mathbf{k}+\mathbf{v}|^2)}{(\varepsilon_S + \frac{1}{2}\nabla^2_{\mathbf{r}_T} - V_{Te} - i\eta)} \phi_{\mathbf{k}+\mathbf{v}}(\mathbf{r}_T) \ , \quad (13)$$

with the electronic scattering energy given by $\varepsilon_S = E - (1/2\nu_i)(\beta\mathbf{K}_f - \mathbf{k} + \mathbf{S})^2 = \frac{1}{2}v^2 + (\mathbf{k}-\mathbf{S})\cdot\mathbf{v} + \varepsilon_f$. Note that $\varepsilon_S - \frac{1}{2}|\mathbf{k}+\mathbf{v}|^2 = \Delta\varepsilon - \mathbf{v}\cdot\mathbf{S}$.

Again, for the interaction region $r_T \lesssim 1/Z_T$ centered around the target nucleus, the off-shell wave function $\psi^-_{\varepsilon,\mathbf{q}}(\mathbf{r}_T)$ of energy ε and momentum $\mathbf{q}$ can be approximated [11] to order $(Z_P/v)^2$ (for the present process) by a target continuum eigenstate $\psi^-_{\mathbf{q}}(\mathbf{r}_T)$ multiplied by an off-shell factor:

$$\psi^-_{\varepsilon,\mathbf{q}}(\mathbf{r}_T) \approx g^-(Z_T^\infty, q, \kappa) \psi^-_{\mathbf{q}}(\mathbf{r}_T) \quad (14)$$

for $\varepsilon \equiv \frac{1}{2}\kappa^2 \approx \frac{1}{2}q^2$. This approximate form is not restricted to a pure Coulomb potential but holds for any modified Coulomb potential. The wave function ϕ_i in the matrix element with its exponential decay at large r_T ensures the validity of the approximation. The factor g^- has the form

$$g^-(Z_T^\infty, q, \kappa) = e^{-\pi\nu_\infty} \Gamma(1 - i\nu_\infty) \left[\frac{q-\kappa}{q+\kappa} \right]^{i\nu_\infty} ; \quad (15)$$

the dependence on the asymptotic form of the target potential is apparent since $\nu_\infty \equiv Z_T^\infty/\kappa$. The gamma function is denoted by $\Gamma(x)$. By way of motivation, a brief discussion of off-shell scattering of a wave packet is given in the Appendix.

Since the Fourier transform of the distortion function is highly peaked about $\mathbf{S} \approx \mathbf{K}_f$, only the $\mathbf{S}$ dependence of $\tilde{D}^-_{\mathbf{K}_f}(\mathbf{S})$ and $\Delta\varepsilon - \mathbf{v}\cdot\mathbf{S}$ in the $\mathbf{S}$ integrand of Eq. (12) need

be retained. Further, when Eq. (13) is approximated as in Eq. (14), the orthogonality of $\psi^-_{\mathbf{k}+\mathbf{v}}(\mathbf{r}_T)$ and $\phi_i(\mathbf{r}_T)$ implies that the U_i term does not contribute to the amplitude Eq. (3). Consequently, the distorted strong-potential Born amplitude in the near-shell approximation takes the form

$$A_{\mathrm{DSPB}}(\mathbf{K}) \approx \int d\mathbf{k}\, \tilde{\phi}_f(\mathbf{k})^* [\gamma^-(Z_T^\infty, q, \kappa)]^* \tilde{V}_{Pe}(\mathbf{k}-\mathbf{K}) \times \langle \psi^-_{\mathbf{k}+\mathbf{v}} | e^{i(\mathbf{k}-\mathbf{K})\cdot\mathbf{r}} | \phi_i \rangle \ , \tag{16}$$

where

$$[\gamma^-(Z_T^\infty, q, \kappa)]^* = (2\pi)^{-3/2}(2q^2)^{i\nu_\infty} e^{\pi\nu_\infty/2}\Gamma(1+i\nu_\infty)\Delta\varepsilon \times \int d\mathbf{S}\, \tilde{D}^-_{\mathbf{K}_f}(\mathbf{S})^* [\Delta\varepsilon - \mathbf{v}\cdot\mathbf{S}]^{-1-i\nu_\infty} \ , \tag{17}$$

with $q=|\mathbf{k}+\mathbf{v}|$, and $\kappa=(v^2+2\mathbf{k}\cdot\mathbf{v}+2\varepsilon_f+i\eta)^{1/2}$ in the definition of ν_∞.

The momentum transfers experienced by the target and projectile ions, respectively, are denoted here by

$$\mathbf{J}=\alpha\mathbf{K}_i-\mathbf{K}_f, \quad \mathbf{K}=\beta\mathbf{K}_f-\mathbf{K}_i \ . \tag{18}$$

Each can be written as the vector sum of a component along $\mathbf{v}$ and a component perpendicular to it. The components parallel to $\mathbf{v}$ are $K_\parallel=-\frac{1}{2}v+(\varepsilon_i-\varepsilon_f)/v$ (for the projectile ion) and $J_\parallel=-\frac{1}{2}v+(\varepsilon_f-\varepsilon_i)/v$ (for the target ion), and the components perpendicular to it are $K_\perp$ for $\mathbf{K}$ and $-K_\perp$ for $\mathbf{J}$. ($\mathbf{J}$ will be used later.) Momentum conservation for the process takes the form $\mathbf{K}+\mathbf{J}+\mathbf{v}=\mathbf{0}$ [25].

The interpretation of Eq. (16) is apparent on making connection with the plane-wave Born approximation for *direct ionization* of an atom. Recall the form of the final scattering wave function for the latter:

$$\langle \mathbf{r}_T, \mathbf{R}_T | \Phi_f \rangle = e^{i\mathbf{K}_f\cdot\mathbf{R}_T} \psi^-_{\mathbf{k}}(\mathbf{r}_T) \ ,$$

with $\psi^-_{\mathbf{k}}$ a continuum eigenstate of the target. The plane-wave Born approximation (PWBA) amplitude is then [26]

$$A_{\mathrm{PWBA}}(\mathbf{Q}) = \tilde{V}_{Pe}(\mathbf{Q}) \langle \psi^-_{\mathbf{k}} | e^{i\mathbf{Q}\cdot\mathbf{r}} | \phi_i \rangle \ ,$$

with $\mathbf{Q}=\mathbf{K}_f-\mathbf{K}_i$. Clearly, except for the off-shell factor γ^-, the picture of capture presented by Eq. (16) involves a folding of the final bound-state momentum distribution with the amplitude for ionization of the electron into the projectile's direction with a comparable velocity. The effect of γ^- is somehow to modulate this folding. In the next section an evaluation will be made which allows a closer look at this connection. In contrast, the full ionization amplitude involves integration over all ejection angles and energies [26].

Integrating over transverse momentum transfers, the total cross section is

$$\sigma = (2\pi v^2)^{-1} \int_0^\infty dK_\perp K_\perp |A(K_\perp)|^2 \ . \tag{19}$$

For capture from the K shell of atoms, σ must be multiplied by a factor of 2 to account for two independent electrons. Capture from the L shell followed by excitation of a K-shell electron into the L-shell hole leads to the same final state. This alternative process is not separately distinguished in the experimental results to which we compare. The contribution is thought to be small, however, owing either to the small L-shell capture cross section at higher energies or to the small excitation cross section at lower energies [3].

III. AMPLITUDE EVALUATION USING ATOMIC POTENTIALS

To obtain a computationally useful form for the amplitude, the off-shell factor γ^- and ionization matrix element need to be evaluated (Secs. III C and III B), and their folding with $\tilde{\phi}_f$ performed. An approximate method of performing the folding is introduced (Sec. III A) which allows a separation of the two above factors. Afterward, each of these is evaluated. Along the way, one must specify the electron–target-ion potential $V_{Te}(r_T)$ and determine the corresponding distorting potential U_f.

A. Transverse-peaking approximation

In considering the near-shell amplitude Eq. (16), observe that for inner-shell capture in an asymmetric collision at intermediate velocities, $k \sim Z_P \ll v$ and $K \sim v$. Further, the amplitude is highly peaked in the forward direction with the major contributions to the total cross section deriving from $K_\perp \lesssim K_\parallel$. It is therefore useful to define cylindrical polar coordinates for $\mathbf{k}$ with $k_\parallel$ parallel to $\mathbf{v}$ and $k_\perp$ perpendicular to it. This allows the introduction of a transverse-peaking approximation [3]: the $k_\perp$ dependence of the $\mathbf{k}$ integrand in Eq. (16) is neglected except in $\tilde{\phi}_f(\mathbf{k})$ and $\Delta\varepsilon$ in γ^-, these factors providing the only rapid variation. Recall that the $1s$ Coulomb wave function in momentum space is $\tilde{\phi}_{1s}(\mathbf{k})=(2^3Z_P^5)^{1/2}/\pi(k^2+Z_P^2)^2$ and that $\Delta\varepsilon=-\frac{1}{2}(k^2+Z_P^2)$, since $\varepsilon_f=-\frac{1}{2}Z_P^2$.

With this approximation and anticipating the form of γ^- given in Eq. (26) below, the $k_\perp$ integration can be performed (as can the corresponding polar-angle integration) to give a factor $E_1[ix(k_\parallel^2+Z_P^2)/2v]$, where the exponential integral function E_1 is defined after Eq. (39). Were γ^- not present in the integrand, a simple $(k_\parallel^2+Z_P^2)^{-1}$ dependence would result, leading, in the complex $k_\parallel$ plane, to poles at $k_\parallel=\pm iZ_P$. As it is, the E_1 function contains essential singularities at the same points. For the upper one, a branch cut can be defined, say along the positive imaginary axis from Z_P to ∞. Additional singularities exist also in the other factors of the $k_\parallel$ integrand. These can be shown to be located in the lower half of the complex plane [3]. Consequently, the integration path along the real $k_\parallel$ axis can be deformed to go around the branch cut. The major contribution to the integral then comes from the vicinity of $k_\parallel=iZ_P$, and since the remaining $k_\parallel$ dependence of the integrand is relative to v or $K_\parallel$ (except for that in E_1), we set $k_\parallel=iZ_P$ in these other factors. The integration of E_1 can then be performed, as is done below in Eq. (38) of Sec. III C. The complete

transverse-peaking approximation consists of setting $\mathbf{k}=iZ_P\hat{\mathbf{v}}$ in all factors of Eq. (16) except the rapidly varying parts $\tilde{\phi}_f(\mathbf{k})$ and $\Delta\varepsilon$. The approximate amplitude is

$$A_{\mathrm{DSPB}}(\mathbf{K})\approx M_{\mathrm{DSPB}}\,A_{IA}(\mathbf{K})\ , \tag{20}$$

where

$$M_{\mathrm{DSPB}}\equiv\frac{\int d\mathbf{k}\,\tilde{\phi}_f(\mathbf{k})^*[\gamma^-(Z_T^\infty,k,\kappa)]^*}{\int d\mathbf{k}\,\tilde{\phi}_f(\mathbf{k})^*}\ , \tag{21}$$

with

$$[\gamma^-(Z_T^\infty,k,\kappa)]^*=(2\pi)^{-3/2}(2\kappa^2)^{i\nu_\infty}e^{\pi\nu_\infty/2}\Gamma(1+i\nu_\infty)\Delta\varepsilon \times\int d\mathbf{S}\,\tilde{D}^-_{\mathbf{K}_f}(\mathbf{S})^*[\Delta\varepsilon-\mathbf{v}\cdot\mathbf{S}]^{-1-i\nu_\infty}\ , \tag{22}$$

and

$$A_{\mathrm{IA}}(\mathbf{K})\equiv\int d\mathbf{k}\,\tilde{\phi}_f(\mathbf{k})^* \times\{\tilde{V}_{Pe}(\mathbf{k}-\mathbf{K})\langle\psi^-_{\mathbf{k}+\mathbf{v}}|e^{i(\mathbf{k}-\mathbf{K})\cdot\mathbf{r}}|\phi_i\rangle\}_{\mathbf{k}=iZ_P\hat{\mathbf{v}}}\ . \tag{23}$$

In Eq. (22), $\nu_\infty=Z_T^\infty/\kappa$ and $\kappa=v+iZ_P$. An important feature of the development consists in the separation of the DSPB amplitude into an IA amplitude (primarily an ionization amplitude) and a momentum-integrated off-shell factor M_{DSPB}. As already noted, this permits one to study the two components separately. Additionally, a test of the quality of the present approximation is shown later in Fig. 5.

B. Ionization matrix element

The matrix element in Eq. (23) is evaluated using a scaled hydrogenic model in which the target potential is $V_{Te}(\mathbf{r}_T)\approx-Z_s/r_T+V_0$, where Z_s is a scaled charge derived using Slater's screening rules, and V_0 is a constant determined by forcing the $1s$ energy for the potential to agree with the experimental value [3]. The use of this model is justified in evaluating the matrix element because the presence of $\phi_i(\mathbf{r}_T)$ effectively restricts the radial integration to the region $r_T\lesssim 1/Z_T$ where the scaled potential agrees to within a few percent with the correct one. While introducing a separate approximation, the use of a scaled potential is not inconsistent with the use of a better potential in the evaluation of M_{DSPB}, for the R integral in the latter relies on large radial values also. It is thus necessary to take into account the correct form of V_{Te}, as is discussed more below. In the scaled model, the matrix element Eq. (23) is [3]

$$\langle\psi^-_{\mathbf{k}+\mathbf{v}}|e^{i(\mathbf{k}-\mathbf{K})\cdot\mathbf{r}}|\phi_i\rangle=4\pi^{1/2}Z_s^{3/2}e^{\pi\nu/2}\Gamma(1+i\nu)\frac{\partial}{\partial Z_s}\left[\frac{(K^2-v^2+Z_s^2+2\mathbf{k}\cdot\mathbf{J}-2iZ_s|\mathbf{k}+\mathbf{v}|)^{-i\nu}}{(Z_s^2+J^2)^{1-i\nu}}\right]\ , \tag{24}$$

where $\nu\equiv Z_s/\kappa$, with κ defined as in Sec. III A. Cross sections obtained using Eq. (24) are compared in Sec. IV B with those obtained from an exact evaluation of Eq. (23).

C. Off-shell factor

To evaluate the integral in Eq. (21) for the integrated off-shell factor M_{DSPB}, the integral representation

$$\Gamma(1+i\nu_\infty)(iA)^{-1-i\nu_\infty}=\int_0^\infty dx\,x^{i\nu_\infty}e^{-ixA}$$

is used to transform $(\gamma^-)^*$ to the form

$$[\gamma^-(Z_T^\infty,k,\kappa)]^*=i(2\kappa^2)^{i\nu_\infty}\Delta\varepsilon \times\int_0^\infty dx\,x^{i\nu_\infty}e^{-ix\Delta\varepsilon}[D^-_{\mathbf{K}_f}(-x\mathbf{v})]^*\ . \tag{25}$$

It is convenient to introduce a new integration variable $u\equiv xv$ to give

$$[\gamma^-(Z_T^\infty,k,\kappa)]^*=i(2|\mathbf{k}+\mathbf{v}|^2/v)^{i\nu_\infty}(\Delta\varepsilon/v) \times\int_0^\infty du\,u^{i\nu_\infty}e^{-iu\Delta\varepsilon/v} \times[D^-_{\mathbf{K}_f}(-u\hat{\mathbf{v}})]^*\ . \tag{26}$$

The many-body aspects of the target-ion–electron interaction are incorporated by using an atomic model potential which is determined by a fit to the Hartree-Fock potential. The total energy of the atom obtained from the energies of the model potential orbitals and their mutual interactions is optimized to best reproduce the total Hartree-Fock energy. The functional form of the atomic model potential is due to Green, Sellin, and Zachor [9,10],

$$V_{Te}(r)=-\frac{1}{r}\left[\frac{Z_T-Z_T^\infty}{He^{r/d}-H+1}+Z_T^\infty\right] \sim\begin{cases}-\dfrac{Z_T}{r} & \text{as } r\to 0\\ -\dfrac{Z_T^\infty}{r} & \text{as } r\to\infty\ .\end{cases} \tag{27}$$

Details of the optimization procedure can be found in Ref. [10]. Table I lists the values of the parameters used in the present work. Also given are the total energy differences from the converged Hartree-Fock values.

The potential Eq. (27) appears in the definition of the distorting potential U_f, Eq. (8b). To obtain an explicit form for U_f, the convolution theorem for the Fourier transform of the product of two functions is used to write

$$U_f(\mathbf{R})=\int d\mathbf{k}\,e^{i\mathbf{k}\cdot\mathbf{R}}\tilde{\rho}(\mathbf{k})\tilde{V}_{Te}(\mathbf{k})\ , \tag{28}$$

TABLE I. Parameters for the model potential fit [Eq. (27)] to the actual atomic potential [10], and error in the corresponding total atomic energy ΔE in parts per million.

Atom	d	H	ΔE (ppm)
C	0.939	2.000	133
Ne	0.558	1.510	42
Ar	1.045	3.660	33

where the functions $\tilde{\rho}$ and $\tilde{V}_{Te}$ are given by

$$\tilde{\rho}(\mathbf{k})=(2\pi)^{-3/2}\int d\mathbf{r}\, e^{-i\mathbf{k}\cdot\mathbf{r}}|\phi_f(\mathbf{r})|^2 , \tag{29}$$

$$\tilde{V}_{Te}(\mathbf{k})=(2\pi)^{-3/2}\int d\mathbf{r}\, e^{-i\mathbf{k}\cdot\mathbf{r}}V_{Te}(\mathbf{r}) . \tag{30}$$

Since $\beta\approx 1$, the β dependence in Eq. (8b) has been neglected, consistent with earlier approximations.

Equation (30) can be evaluated by means of formula 3.411.6 of Ref. [27] while Eq. (29) is easily found with the replacement $Z\rightarrow 2Z$ in $\tilde{\phi}_{1s}(\mathbf{k})$ and suitable normalization of the result. One obtains

$$\tilde{V}_{Te}(\mathbf{k})=\left(\frac{2}{\pi}\right)^{1/2}\left\{-\frac{a}{c}\sum_{m=1}^{\infty}(-c)^m\left[k^2+\left[\frac{m}{d}\right]^2\right]^{-1}-\frac{Z_T^{\infty}}{k^2}\right\} , \tag{31}$$

$$\tilde{\rho}(\mathbf{k})=2^{5/2}Z_P^4\pi^{-3/2}[(2Z_P)^2+k^2]^{-2} . \tag{32}$$

In Eq. (31), $c\equiv -1+1/H$. Inserting these expressions into Eq. (28) and reducing the power of the denominator in $\tilde{\rho}$ by use of a parametric differentiation with respect to Z_P, formulas 3.725.1 and 3.728.2, respectively, of Ref. [27] allow one to evaluate the first and second terms arising from the two terms in $\tilde{V}_{Te}$ to give

$$U_f(R)\equiv\frac{F(R)}{R} , \tag{33}$$

with

$$F(R)=-4Z_P^3\frac{\partial}{\partial Z_P}\left[\frac{a}{2c}\sum_{m=1}^{\infty}(-c)^m\frac{e^{-2Z_PR}-e^{-mR/d}}{(m/d)^2-(2Z_P)^2}-\frac{Z_T^{\infty}}{8Z_P^2}\{1-e^{-2Z_PR}\}\right] . \tag{34}$$

Substituting Eqs. (34) and (26) into Eq. (21) for the integrated off-shell factor M_{DSPB}, and introducing also a new integration variable $W\equiv R/u$ into the eikonal integral in $D^-_{\mathbf{K}_f}$, the factor can be written

$$M_{\mathrm{DSPB}}=\frac{i}{v}\int_0^{\infty}du\, Q(u)e^{-iI(u)/v} , \tag{35}$$

where the functions $Q(u)$ and $I(u)$ are defined as

$$I(u)=\int_1^{\infty}\frac{dW}{W}[F(uW)+Z_T^{\infty}] \tag{36}$$

and

$$Q(u)=\int d\mathbf{k}\,\tilde{\phi}_f(\mathbf{k})^*\tfrac{1}{2}(k^2+Z_P^2)\times\exp[-iu(k^2+Z_P^2)/2v] . \tag{37}$$

Note that there is a complete separation of the integration over the bound-state momentum $\mathbf{k}$ and the part of the distortion D^- function which is dependent on the short-range part of the distorting potential represented by the exponential in Eq. (6). Already in arriving at this equation, however, factors from the Coulomb part of the heavy-particle motion have canceled factors arising from the electron off-shell factor γ^-. This separation is at the expense of a convolution of $Q(u)$ and $\exp[-iI(u)/v]$ which represents the interaction of the electronic and heavy-particle motions.

If the specific form for the bound-state wave function is inserted into Eq. (21) and the angular integrations are performed, one obtains the result

$$Q(u)=(2Z_P)^{5/2}\int_0^{\infty}dk\,k^2(k^2+Z_P^2)^{-1}\times\exp[-iu(k^2+Z_P^2)/2v] . \tag{38}$$

This integral gives the complex error function Φ as formula 3.466.2 of Ref. [27] shows. The result is

$$Q(u)=2^{3/2}\pi Z_P^{7/2}\{\Phi[\tfrac{1}{2}Z_P(1+i)\sqrt{u/v}\,]-1+Z_P^{-1}(1-i)\sqrt{v/\pi u}\,e^{-iZ_P^2u/2v}\} . \tag{39}$$

In terms of the exponential integral

$$E_1(z)\equiv\int_1^{\infty}\frac{dW}{W}e^{-zW}$$

and the function $E_0(z)\equiv e^{-z}/z$, $I(u)$ can be expressed as

$$I(u)=4Z_P^3\left[\frac{a}{2c}\sum_{m=1}^{\infty}(-c)^m\left[\frac{2uE_0(2Z_Pu)}{(m/d)^2-(2Z_P)^2}-8Z_P\frac{E_1(2Z_Pu)-E_1(mu/d)}{[(m/d)^2-(2Z_P)^2]^2}\right]\right]+Z_T^{\infty}Z_P\left[uE_0(2Z_Pu)+\frac{E_1(2Z_Pu)}{Z_P}\right] . \tag{40}$$

The integrand in Eq. (35) is highly oscillatory and of a form for both $u\rightarrow 0$ and $u\rightarrow\infty$ that barely leads to convergence of the integral. Equation (35) is evaluated numerically [28] by employing the technique of explicitly subtracting the small and large u leading forms of the integrand and then adding their contributions separately. A much more well-behaved integrand is then obtained, leading to relatively better numerical convergence. Re-

sults reported here are converged to within 0.01%.

For reference purposes, note that if V_{Te} is approximated by a scaled potential as discussed above in Sec. III B, then $\gamma^- = g^-$ is obtained. Using this result in the *undistorted* version of the theory, the off-shell factor can be shown to have the form [3]

$$|M_{\mathrm{SPB}}|^2 = \frac{2}{(1+e^{-2\pi\nu})(1+\nu^2)} \tag{41}$$

in the so-called full-peaking evaluation of the amplitude, obtained by setting $\mathbf{k}=\mathbf{0}$ in the integrand except for the $k^2+Z_P^2$ dependence. Also, $\nu = Z_T/v$ is used instead of ν_∞. Since $\nu \approx 1$ at the matching velocity $v \approx Z_T$, implying that $e^{-2\pi\nu} \ll 1$, we have $|M_{\mathrm{SPB}}|^2 \approx 1$. That is, at the matching velocity relative to Z_T, the off-shell effects vanish.

IV. RESULTS AND DISCUSSION

In this section calculated K-shell electron capture cross sections for protons incident on carbon, neon, and argon atoms are presented. Experimental K-shell binding energies are used in the definition of the minimum momentum transfers $K_\parallel$ and $J_\parallel$, and in the scaling of the impact velocity noted in the figure captions. The experimental energies used [23] for carbon, neon, and argon are, respectively, 288, 870.2, and 3206 eV. Section IV A presents a comparative discussion of the magnitudes of the off-shell effects for the atoms relative to each other and to the undistorted SPB values. In Sec. IV B, DSPB cross sections are compared with experimental and other theoretical results.

A. Off-shell effects

In Fig. 1 the ratio of the DSPB total K-shell capture cross section to the IA cross section for protons on carbon, neon, and argon is shown versus the scaled impact velocity v. The velocity is scaled by the target K-shell orbital velocity, defined as $v_T \equiv (\varepsilon_K/13.606)^{1/2}$ where the experimental K-shell binding energy ε_K is given in eV. The range of velocities plotted for each atom generally brackets the available experimental data. The behavior of the curves is comparatively smooth and similar in each case. At large velocities, the curves approach unity showing that off-shell effects become negligible. Beyond the peak in the cross section which occurs near $v/v_T \approx 1$, it is seen that the impulse approximation is valid to good approximation, particularly for higher asymmetry. As the velocity decreases, however, the off-shell effects increase in magnitude. Mostly, as the asymmetry decreases, the effects become more pronounced. Smaller velocities imply smaller minimum momentum transfers and less deep probing of the electron–target-ion interaction. To whit, the screening effects increase. Over the whole velocity range shown, the off-shell effects are seen to be barely more than 15% in argon and 25% in neon. For

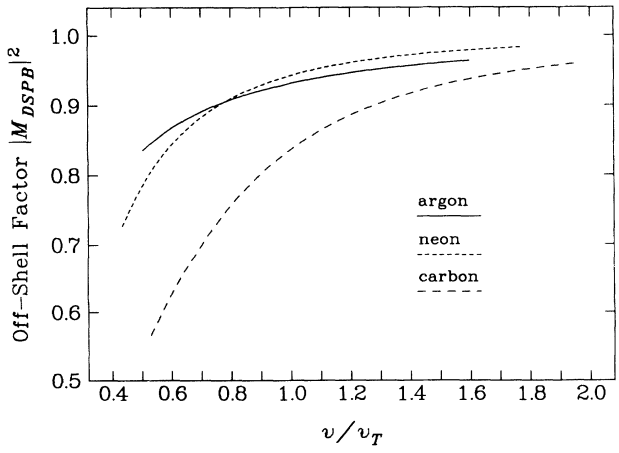

FIG. 1. Ratio of DSPB total K-shell capture cross section to IA cross section for protons on carbon, neon, and argon versus scaled impact velocity v. The velocity is scaled by the target K-shell orbital velocity, defined as $v_T \equiv (\varepsilon_K/13.606)^{1/2}$ with the experimental K-shell binding energy ε_K given in eV.

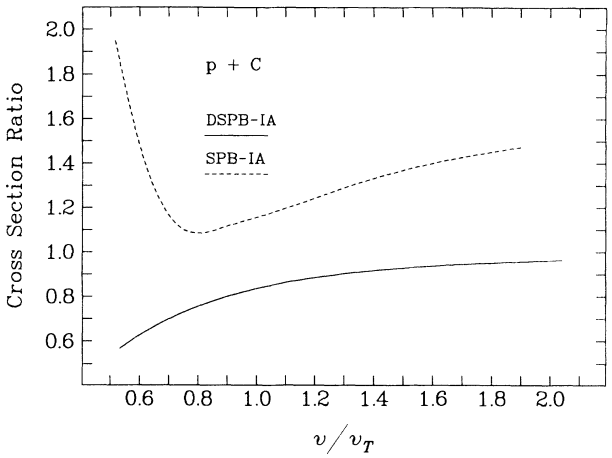

FIG. 2. Ratios of DSPB and SPB [3] total K-shell capture cross sections to IA cross section for protons on carbon versus scaled impact velocity v, defined as for Fig. 1.

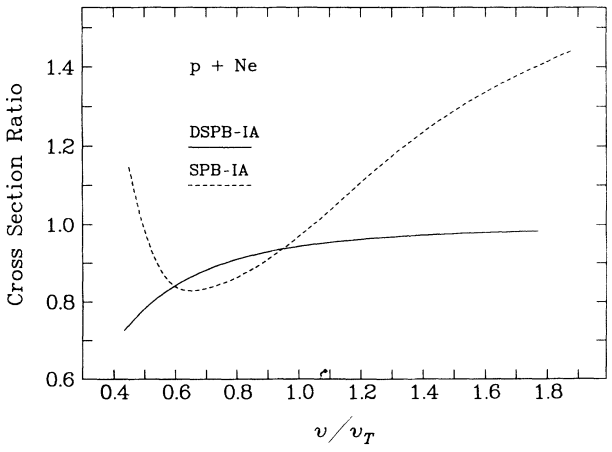

FIG. 3. Ratios of DSPB and SPB [3] total K-shell capture cross sections to IA cross section for protons on neon versus scaled impact velocity v, defined as for Fig. 1.

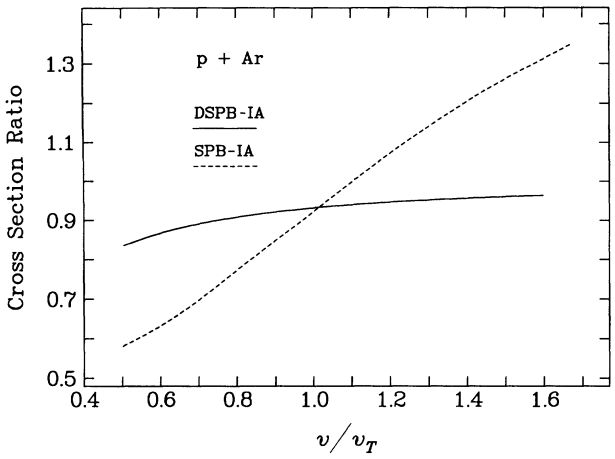

FIG. 4. Ratios of DSPB and SPB [3] total K-shell capture cross sections to IA cross sections for protons on argon versus the scaled impact velocity v, define as for Fig. 1.

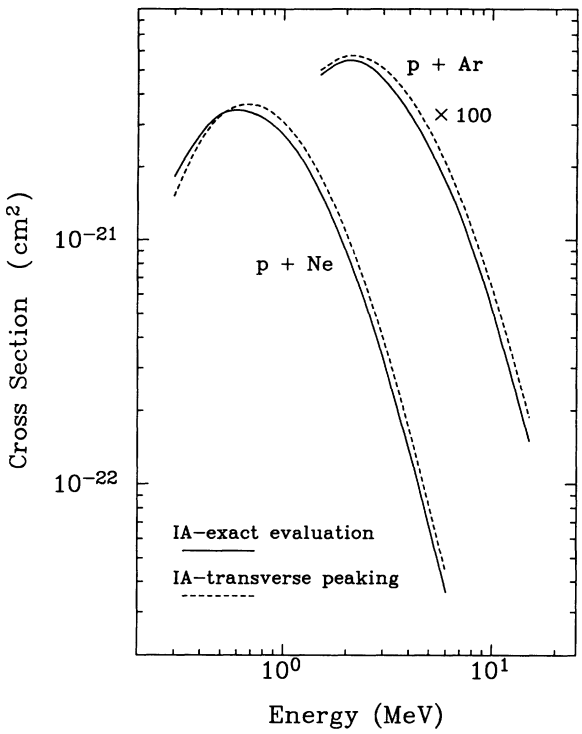

FIG. 5. IA total K-shell capture cross sections for proton impact on neon and argon atoms. In a scaled hydrogenic model, the amplitude is evaluated exactly [28] and in a transverse-peaking approximation [3].

carbon, the effects are generally larger, up to 40%. In this case, however, the lower impact velocities are rather small: for $v/v_T=0.6$, $v=2.76$ a.u.

Interestingly, the magnitude of the off-shell effect for one atom is not uniformly greater than that for another atom with smaller nuclear charge. In particular, the effect in argon are slightly larger than the neon ones at scaled velocities greater than about 0.8. This is most likely attributable to a considerably larger screening effect in argon (with eight electrons). The increased effects of the screening for *lower* velocities eventually take over, however, and the off-shell effects in neon then become larger than for argon.

We compare in Figs. 2–4 the off-shell effects arising in the DSPB theory with those arising in the undistorted theory (SPB) for each atom, respectively. The results are once again plotted versus the scaled velocity. In all cases, it is seen that the effects in the undistorted theory are, on the whole, much larger and increase both for small and large velocities. For carbon and neon, the effects reach a minimum in the vicinity of the matching velocity while for argon they continually decrease. It would seem, however, in view of Figs. 2 and 3 that at still lower velocities than are shown in Fig. 4, the argon effects would reach a minimum and then increase also. The fact that the effects in the SPB theory do not disappear (that is, the ratio equals unity) when the scaled velocity equals one, as Eq. (41) implies, derives partly from our use of transverse-peaking results in the figures versus a full-peaking approximation in Eq. (41), and partly from the different scaling of the velocity, by $v_T \neq Z_T$, in the figures.

B. Total K-shell cross sections

In the present work we have emphasized how the off-shell effects are altered in the DSPB theory versus the SPB theory. Still, the final determination of the total cross section rests on an evaluation of the IA cross section, since we have shown the DSPB cross section to be the product of an off-shell factor and an IA cross section. Figure 5 presents IA total K-shell capture cross sections for proton impact on neon and argon targets. Within the framework of a scaled hydrogenic model, a comparison is shown of results obtained when the amplitude Eq. (23) is evaluated exactly [29] and in the transverse-peaking approximation [3] used in the present work. It is seen both for neon and argon that the transverse-peaking cross sections agree excellently in shape with the exact cross sections, and that their magnitudes are generally too large by at most 20%. If the exact cross sections were used in the comparison with experiment below, even better agreement would be found than is shown. However, we maintain a consistent treatment and employ our transverse-peaking results. Similar screened-hydrogenic cross sections for carbon are not available for comparison. We conclude that the transverse-peaking approximation is therefore justified for the present discussion.

We compare in Figs. 6–8 our calculated DSPB total K-shell capture cross sections for protons on carbon, neon, and argon with experimental and other theoretical results. In Fig. 6 for carbon, the experimental results are those of Cocke and co-workers [12] and the theoretical results are from the continuum distorted-wave theory of Belkić, Gayet, and Salin [16], the renormalized SPB approximation of Marxer and Briggs [18], and the coupled-Sturmian-pseudostate calculation of Winter [19]. The theoretical results are for $1s \rightarrow 1s$ capture only while the experimental results include capture to all final states. For the coupled-state work, the values given in Table V of Ref. [19] have been averaged. It is seen that agreement

with experiment is rather good at the higher velocities, particularly so, taking into account the excited-state capture component which is thought to be about 20%. At the lower velocities, the DSPB results are somewhat high, but the excited-state part is harder to estimate, and the approximations used in the DSPB amplitude are less well justified because of the low absolute magnitude of the velocity.

The renormalized SPB theory is seen also to give good agreement with the data, being slightly high at the higher velocities and low at the lower velocities. The shape of the RSPB curve seems to be too broad while the DSPB curve agrees better, although it is shifted somewhat to the low-velocity side. The RSPB theory [18] improves on the SPB theory by correcting for a loss of normalization suffered by the off-shell scattering state [Eq. (13) with S omitted]. While the justification of the need for renormalization is certainly valid, the manner of introduction of the correction is not grounded in the formal theory of scattering, and the rather approximate evaluation of it contrasts with an otherwise exact treatment of the SPB amplitude. Still, the agreement with the experimental results in the carbon case (and neon and argon below) is good. The differences between the DSPB and RSPB results are generally the same for carbon, and neon and argon (below), the RSPB results being lower at the low velocities and higher at the high velocities.

The agreement of the DSPB cross sections with the coupled-Sturmian results of Winter [19] is quite good. This is especially notable since the same model target potential and experimental binding energy are employed in both calculations. The convergence of the results of coupled-channels and perturbative treatments with each other and with experiment is particularly encouraging. Also shown in Fig. 6 are the CDW result which rapidly become too high as the energy decreases, as is expected according to the validity criterion of the theory [17]. Somewhat surprisingly, though, the RSPB and CDW results are virtually identical at high energies.

In Fig. 7 for neon, the experimental results are from Cocke *et al.* [13] and Rødbro *et al.* [12], and the theoretical results are from the renormalized SPB approximation [18] and the coupled-Sturmian-pseudostate calculation of Winter [20]. The experimental results include capture to all final states. The comments on the agreement between the DSPB results and experiment for the carbon target are generally valid for the neon case also. The overall agreement in the neon case is, however, somewhat better. This fact most probably results from the smaller errors in our approximations due to the greater asymmetry of the collision ($Z_P/Z_T=1/10$) and the greater magnitude of the velocities involved. The RSPB results likewise show comparable agreement with experiment as for carbon, though the cross section is somewhat high for the larger

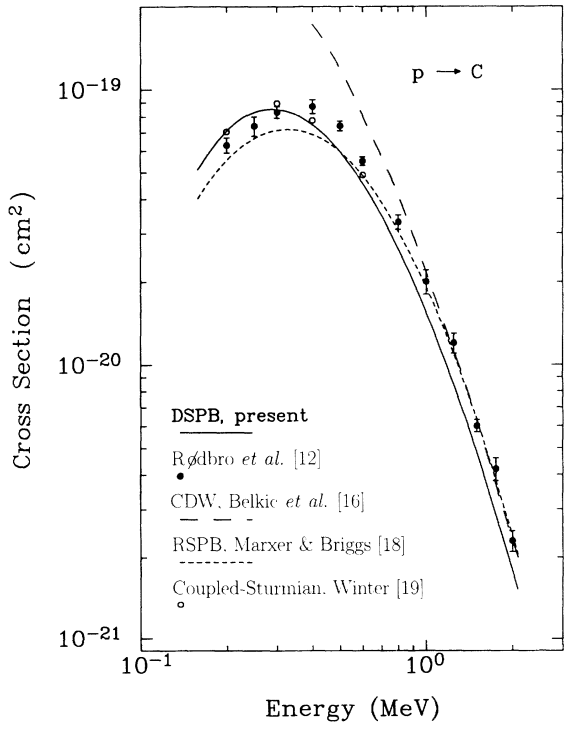

FIG. 6. Total K-shell capture cross section for protons on carbon versus impact energy E. Experimental results: Rødbro *et al.* [12]. Theoretical results: DSPB, present work; continuum distorted wave (CDW), Belkić, Gayet, and Salin [16]; renormalized SPB (RSPB), Marxer and Briggs [18]; coupled Sturmian pseudostate, Winter [19]. The experimental results include capture to all final states.

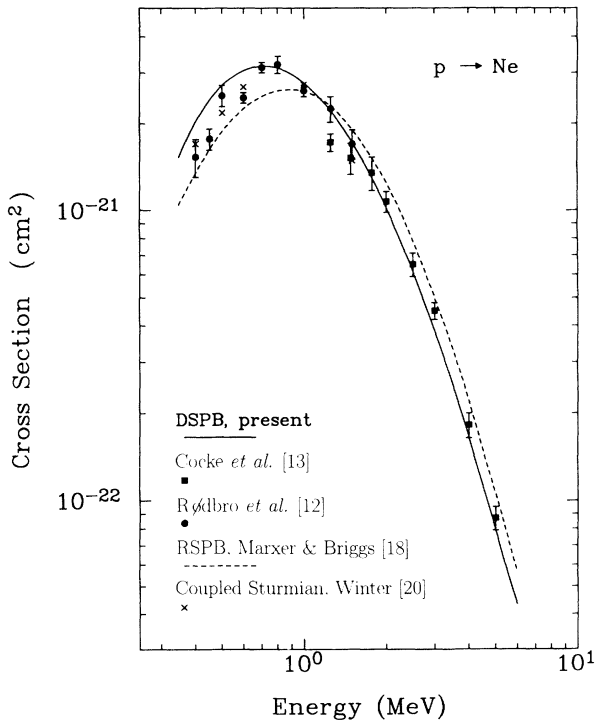

FIG. 7. Total K-shell capture cross section for protons on neon versus impact energy E. Experimental results: Cocke *et al.* [13]; Rødbro *et al.* [12]. Theoretical results: DSPB, present work; renormalized SPB, Marxer and Briggs [18]; coupled Sturmian pseudostate, Winter [20]. The experimental results include capture to all final states.

velocities.

The agreement of the DSPB cross sections with the coupled-Sturmian results of Winter [20] is good, although relative to carbon, the DSPB neon results are slightly higher than the Sturmian results. Here also, the same model target potential and experimental binding energy have been employed in the two calculations. The Sturmian results for neon, as for carbon, represent an average of the results obtained using three bases of progressively larger size. The range of the three values for a given energy is somewhat larger for neon than for carbon [20]. Still, the good agreement of the coupled-channels and perturbative treatments with each other and with experiment is encouraging.

Figure 8 for argon shows, in addition to the DSPB results, experimental results from Macdonald, Cocke, and Eidson [14] and Horsdal-Pedersen *et al.* [15] and other theoretical results including those from the continuum distorted-wave theory of Belkić and McCarroll [17], the RSPB approximation [18], and the coupled-channels (CC) calculations of Ford *et al.* [21]. The experimental results include capture to all final states. The comments on the agreement between the DSPB results and experiment for neon are equally valid for the argon case. Overall agreement for argon is excellent at the high velocities, but the present results are slightly high for the lower velocities. The good agreement again results from the smaller errors in our approximations due to the greater asymmetry of the collision ($Z_P/Z_T=1/18$) and the large velocities involved. The RSPB results similarly show the same agreement with experiment as for neon; the cross section is somewhat high for the larger velocities. The coupled-channel results presented in Fig. 8 tend to agree with the present theoretical results, except the highest-velocity data point which is too high and the lowest-velocity point which is very low. Finally, the CDW results shown in Fig. 8 are, except at the low- and high-velocity limits of the data, too low, and exhibit structure at intermediate velocities not reproduced in the data. At high energies, the DSPB and CDW results appear to converge although the curves could simply be crossing each other.

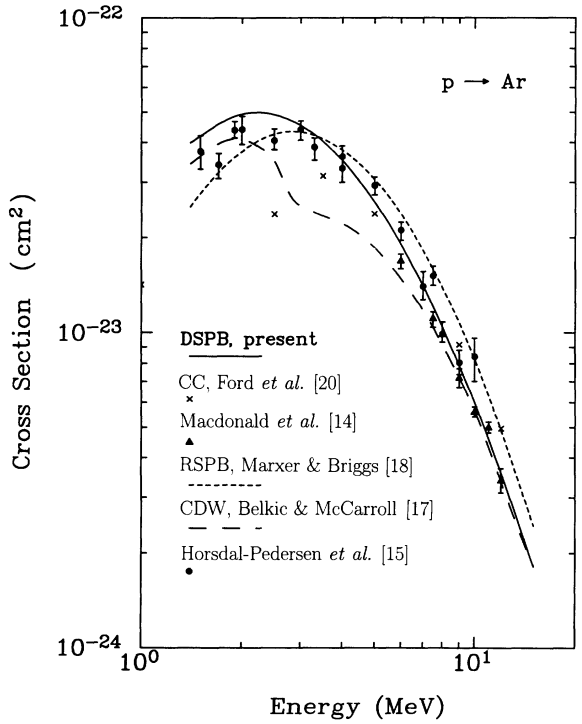

FIG. 8. Total K-shell capture cross section for protons on argon versus impact energy E. Experimental results: Macdonald, Cocke, and Eidson [14]; Horsdal-Pedersen *et al.* [15]. Theoretical results: DSPB, present work; continuum distorted wave (CDW), Belkić and McCarroll [17]; renormalized SPB, Marxer and Briggs [18]; coupled channels (CC), Ford *et al.* [21]. The experimental results include capture to all final states.

V. CONCLUSION

In summary, it has been shown that, in contrast with the undistorted strong-potential Born approximation, inclusion of an accurate representation of the electron–target-ion interaction in the distortion potential, and thus in the description of the distorted heavy-particle motion itself, leads to radically different off-shell effects in the total K-shell capture cross section. The cross sections obtained with the distorted theory are in quite good agreement with the experimental data and, overall, the agreement is considerably better than that of the original undistorted SPB theory. Significant improvement is obtained over results of other perturbative theories, except for the renormalized SPB approximations which, however, is not based entirely consistently on formal scattering theory. The simple picture of inner-shell capture involving ionization of the electron from the target followed by attachment to the projectile is maintained while a more accurate and well-founded treatment is employed, taking full account of the anomalies of Coulomb scattering.

It has been argued here that the transverse-peaking approximation introduces generally small errors in the amplitude, but to obtain a complete picture of the distorted strong-potential Born approximation, better evaluations of the ionization matrix element and off-shell factor need to be performed without the factorization effected here, together with a more accurate treatment of the longitudinal components and, perhaps, the transverse components. Only then can one fully judge how valid a representation of inner-shell capture the DSPB approximation provides. This calculation is currently under investigation.

ACKNOWLEDGEMENTS

I would like to thank Professor T. G. Winter for making his neon results available before publication. This work is supported by the U.S. Department of Energy, Office of Energy Research, Office of Basic Energy Sciences, Division of Chemical Sciences. Calculations were performed on the Lawrence Livermore National Laboratory Cray-2 and the Pennsylvania State University IBM 3090-600S supercomputers.

APPENDIX: OFF-ENERGY-SHELL SCATTERING

While the concept of off-the-energy-shell scattering arises naturally in the theory of scattering amplitudes for rearrangement processes, it is perhaps worthwhile to outline an intuitive picture of off-energy-shell scattering in a time-dependent development. Consider the final bound state of the captured electron in the frame of the projectile. To express this state in the target frame in a nonrelativistic treatment, it is necessary to perform a Galilean boost of it. If, in addition, the coordinate space representation of this state is Fourier analyzed as

$$\phi_f(\mathbf{r}_P)e^{-i\varepsilon_f t}=(2\pi)^{-3/2}\int d\mathbf{k}\,\tilde{\phi}_f(\mathbf{k})e^{i(\mathbf{k}\cdot\mathbf{r}_P-\varepsilon_f t)},$$

one finds in the target frame the new function (denoted with an overbar)

$$\bar{\phi}_f(\mathbf{r}_T)e^{-i\varepsilon_f t}=e^{i\{\mathbf{v}\cdot\mathbf{r}_T-[(1/2)v^2+\varepsilon_f]t\}}\phi_f(\mathbf{r}_T-\mathbf{v}t)$$
$$=(2\pi)^{-3/2}\int d\mathbf{k}\,\tilde{\phi}_f(\mathbf{k})e^{i[(\mathbf{v}+\mathbf{k})\cdot\mathbf{r}_T-\varepsilon(\mathbf{k})t]},$$

where $\varepsilon(\mathbf{k})\equiv\frac{1}{2}v^2+\mathbf{v}\cdot\mathbf{k}+\varepsilon_f$. In effect, this wave function represents the electron as a packet (centered around the projectile) of traveling plane-wave states of index $\mathbf{k}$ and momentum $\mathbf{k}+\mathbf{v}$. The corresponding energy (that is, the factor multiplying t in the exponential) of each component is $\varepsilon(\mathbf{k})$. However, this energy is not the same as that of the plane-wave component. The difference is

$$\Delta\varepsilon=\tfrac{1}{2}(\mathbf{v}+\mathbf{k})^2-\varepsilon=\tfrac{1}{2}k^2-\varepsilon_f,$$

and it never equals zero.

Off-shell scattering arises generally in any type of rearrangement collision, where an active particle is transferred from one frame to another relatively moving frame. The nonuniform effects encountered in the present work as the energy shell is approached, i.e., as $\Delta\varepsilon\to 0$, result from the long-range r^{-1} behavior of the Coulomb potential.

We can judge the order of magnitude of the energy difference by noting that as a result of the presence of $\tilde{\phi}_f(\mathbf{k})$ in the integrand, the bound-state momentum $\mathbf{k}$ has the order of magnitude $k\sim Z_P$, implying that $\Delta\varepsilon\sim Z_P^2$. The energy ε has the order of magnitude $\varepsilon\sim v^2$. Consequently, the energy defect is small:

$$\Delta\varepsilon\ll\varepsilon\ .$$

This then is the justification of our near-shell approximation.

If the time evolution of this state under the influence of a potential V is considered, the resulting wave function can be shown to be a solution of an *inhomogeneous* Schrödinger equation:

$$\left\{-\frac{\hbar^2}{2}\nabla_{\mathbf{r}}^2+V(\mathbf{r})-\varepsilon\right\}\psi^-_{\varepsilon,\mathbf{k}+\mathbf{v}}(\mathbf{r})=\Delta\varepsilon e^{i(\mathbf{k}+\mathbf{v})\cdot\mathbf{r}}\ .$$

This wave function is identical to the one defined by Eq. (13). Indeed, Eq. (13) is obtained by operator manipulation of this inhomogeneous Schrödinger equation.

[1] J. Macek and K. Taulbjerg, Phys. Rev. Lett. **46**, 170 (1981); D. H. Jakubassa-Amundsen, J. Phys. B **14**, 2647 (1981); N. C. Sil and J. H. McGuire, J. Math. Phys. **26**, 845 (1985); J. Macek and X. Y. Dong, Phys. Rev. A **38**, 3327 (1988).

[2] J. S. Briggs, J. Phys. B **10**, 3075 (1977); D. H. Jakubassa-Amundsen and P. A. Amundsen, Z. Phys. A **297**, 203 (1980); P. A. Amundsen and D. H. Jakubassa, J. Phys. B **13**, L467 (1980).

[3] J. Macek and S. Alston, Phys. Rev. A **26**, 250 (1982); S. Alston, *ibid.* **27**, 2342 (1983).

[4] S. Alston, Phys. Rev. A. **38**, 3124 (1988).

[5] D. P. Dewangan and J. Eichler, J. Phys. B **18**, L65 (1985).

[6] J. Macek, J. Phys. B **18**, L71 (1985); J. H. McGuire, *ibid.* **18**, L75 (1985).

[7] J. Macek and K. Taulbjerg, Phys. Rev. A **39**, 6064 (1989); J. Phys. B **22**, L523 (1989).

[8] K. Taulbjerg, R. O. Barrachina, and J. H. Macek, Phys. Rev. A **41**, 207 (1990).

[9] A. E. S. Green, D. L. Sellin, and A. S. Zachor, Phys. Rev. **184**, 1 (1969).

[10] P. P. Szydlik and A. E. S. Green, Phys. Rev. A **9**, 1885 (1974).

[11] S. Alston, Phys. Rev. A **38**, 636 (1988).

[12] M. Rødbro, E. Horsdal-Pedersen, C. L. Cocke, and J. R. Macdonald, Phys. Rev. A **19**, 1936 (1979).

[13] C. L. Cocke, R. K. Gardner, B. Curnutte, T. Bratton, and T. K. Saylor, Phys. Rev. A **16**, 2248 (1977).

[14] J. R. Macdonald, C. L. Cocke, and W. W. Eidson, Phys. Rev. Lett. **32**, 648 (1974).

[15] E. Horsdal-Pedersen, C. L. Cocke, J. L. Rasmussen, S. L. Varghese, and W. Waggoner, J. Phys. B **16**, 1799 (1983).

[16] Dž. Belkić, R. Gayet, and A. Salin, Phys. Rep. **56**, 279 (1979).

[17] Dž. Belkić and R. McCarroll, J. Phys. B **10**, 1933 (1977).

[18] H. Marxer and J. S. Briggs, J. Phys. B **25**, 3823 (1992).

[19] T. G. Winter, Phys. Rev. A **47**, 264 (1993).

[20] T. G. Winter (private communication).

[21] A. L. Ford, R. L. Becker, G. L. Swafford, and J. F. Reading, J. Phys. B **12**, L491 (1979).

[22] C. J. Joachain, *Quantum Collision Theory* (North-Holland, Amsterdam, 1975).

[23] M. O. Krause, Oak Ridge National Laboratory Report No. ORNL-TM-2943, 1970 (unpublished).

[24] L. D. Faddeev, Zh. Eksp. Teor. Fiz. **39**, 1454 (1960) [Sov. Phys. JETP **12**, 1014 (1961)].

[25] S. Alston, Phys. Rev. A **42**, 331 (1990).

[26] D. H. Madison and E. Merzbacher, in *Atomic Inner-Shell Processes, Vol. 1, Ionization and Transition Probabilities,* edited by B. Crasemann (Academic, New York, 1975), p. 1.

[27] I. S. Gradshteyn and I. M. Ryzhik, *Tables of Integrals, Series, and Products* (Academic, New York, 1980).

[28] G. E. Forsythe, M. A. Malcolm, and C. B. Moler, *Computer Methods for Mathematical Computations* (Prentice-Hall, Englewood Cliffs, NJ, 1977), Chap. 5.

[29] D. H. Jakubassa-Amundsen and P. A. Amundsen, J. Phys. B **14**, L705 (1981).